Alma Mater Studiorum · University of Bologna

School of Science
Department of Physics and Astronomy
Master Degree in Physics

Thermodynamics of hydrogen absorption in Mg thin films and multilayers studied by electrochemical method

Supervisor:
Prof. Luca Pasquini

Co-supervisors:
Dr. Stefan Wagner
Prof. Astrid Pundt

Submitted by:
Dario Verna

Academic Year 2021/2022

Abstract

Electrochemical hydrogen loading is a technique used to produce and study the hydrogenation in metals starting from a liquid solution containing water. It is a possible alternative to another, well-established technique which loads hydrogen starting from its gas phase. In this work, the electrochemical method is used to understand the fundamental thermodynamics of hydrogen loading in constraint systems such as thin films on substrates, and possibly distinguish the role of interfaces, stresses and microstructure during the hydrogenation process. The systems under study are thin films of Pd, Mg/Pd, and Ti/Mg multilayers. Possible future technological applications may be in the field of hydrogen storage and hydrogen sensors. Towards the end, the experimental setup is modified by introducing an automatic relay. This change leads to improvements in the data analysis and in the attainable information on the kinetics of the systems.

Contents

Introduction

Hydrogen is a energy carrier with a very high energy density (about 120 MJ/kg[1]). Hydrogen produced using renewable energy has the potential of being an important way of storing energy in the future. Mg and Mg-Ti thin films are systems of interest for applications in this field because they change their structure and optical properties upon hydrogen absorption. This property can be applied in hydrogen sensors and smart absorbers [2]. Moreover, the films serve as model systems to study the thermodynamics of alloys with constraint conditions. In this work the hydrogenation of such system is investigated using an electrochemical setup, rather than the more well-established gas phase loading. In particular, this works aims at delivering the same thermodynamic information as the typical measure of gas phase loading, called the Pressure Composition Isotherm (PCI), by directly measuring the hydrogen concentration and the electrochemical voltage within the electrochemical cell, while also measuring in-situ the optical transmittance of the samples. With electrochemistry it is possible to get even more information, as one can study how the chemical potential changes when a defined amount of hydrogen diffuses in the sample and stresses relax. This is not possible for gas phase loading, where the chemical potential is fixed. The long-term goal of the project is to use the electrochemical method in order to be able to distinguish the role of interfaces, stresses and microstructure during hydrogen loading. To achieve this, different parameters need to be adjusted such as the applied voltage, the pulse duration and the waiting time between pulses.

This work is divided in three main chapters: Chapter 1 gives a synthetic presentation of the results on hydrogen in metals which are relevant for this study; Chapter 2 describes the technique used to produce the sample and the experimental setup of electrochemical hydrogen loading; Chapter 3 shows the results of various types of measures performed on the produced samples, followed by data interpretation.

Chapter 1

Hydrogen-Metal systems

1.1 Hydrogen in bulk metals

1.1.1 Hydrogen absorption

The first step for hydrogen intake inside of a metal is the adsorption on its surface. Adsorption can be of two kinds: it is called physisorption when the hydrogen gas molecules stick to the surface due to van der Waals forces; its called chemisorption when chemical bonds change to include the adsorbate [4]. In the case of hydrogen, chemisorption is dissociative, meaning the diatomic molecule H_2 dissociates into atomic H. This process takes place on the surface of the metal. The two energy profiles of the dissociated and undissociated hydrogen are shown in Figure 1.1, from [3]. On the left, sufficiently far from the metal surface, the most energetically favourable configuration is with gaseous hydrogen, with energy set to zero. If the gas molecule is closer, van der Waals forces can trap it on the surface. The most energetically favourable configuration is the dissociation of the hydrogen molecule on the metal surface. Despite this, dissociation is not always what is observed, due to the presence of an energetic barrier at the transient state which can hinder dissociation. If the metal dissolves hydrogen, it can spontaneously form a compound by absorbing it inside the crystal structure if the reaction is exothermic. Otherwise, the system may need additional energy for the absorption to happen. These two different scenarios are illustrated by the two curves on the right. Inside the metal, the energy profile depends on the distribution of the host atoms.

1.1.2 Lattice expansion

When hydrogen is absorbed inside a metal like palladium, it occupies the interstitial sites, causing crystal lattice distortion. If a host metal atom occupies a mean volume Ω and one hydrogen atom causes a volume change Δv, then the stress field produced will depend on the ratio $\Delta v/\Omega$. We can known this quantity by measuring the volume

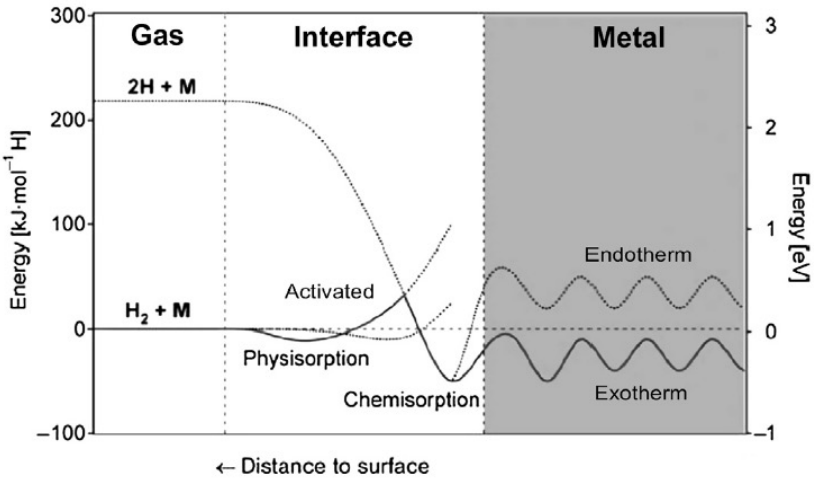

Figure 1.1: Energy diagram of the hydrogen gas absorption process. On the left, distant from the surface, the most favourable condition is for the hydrogen to form diatomic gas molecules. The energy of this configuration is set to zero. In this case hydrogen dissociation is far more unlikely to happen. In the center, closer to the surface, the gas molecules are weakly trapped via van der Waals forces, shown by the typical Lennard-Jones potential profile. For the hydrogen to get even closer, dissociation into hydrogen atoms has to happen. On the right, inside the metal, two possibilities arise. If the reaction is exothermic absorption will happen, causing release of heat. Otherwise, the system may need additional energy for the absorption to happen. From [3].

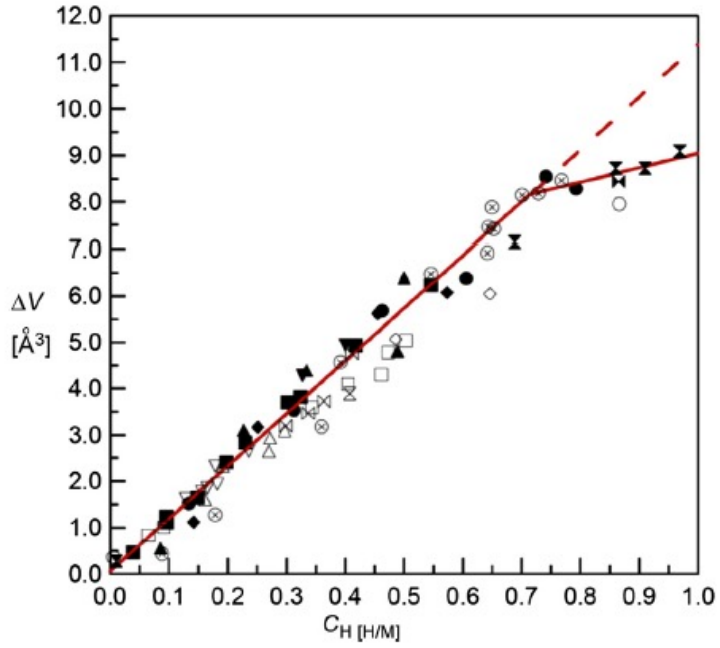

Figure 1.2: Expansion of the unit cell of different fcc metals and alloys upon hydrogen absorption. Up to very high concentrations, the change is linear. The slope in the linear range is $\Delta V/c_H = 11.5$ Å^3, which is the increase in the unit cell volume after the intake up to four hydrogen atoms. This means the volume difference caused by one hydrogen atom is $\Delta v = 2.8$ Å^3. From [6].

change ΔV of the initial volume V, using Equation (1.1):

$$\frac{\Delta V}{V} = \frac{N_{\mathrm{H}} \Delta v}{N \Omega} = c_{\mathrm{H}} \frac{\Delta v}{\Omega} \tag{1.1}$$

where N_{H} is the number of hydrogen atoms and N the number of host metal atoms. The collection of experimental results from this type of measurement and other techniques gives the value $\Delta v/\Omega = 0.19 \pm 0.01$ for palladium [5]. Baranowski et al. [6] have collected the data of unit cell expansion ΔV for many fcc host metals and found that the change is linear over a wide concentration range. The result are shown in Figure 1.2.

For nanomaterials, the situation is more complicated than the free bulk, since the free expansion is often hindered in certain directions. Also plastic deformation has to be taken into account [4].

	P(mbar)	H/M	wt.%	ΔH(kJ molH_2^{-1})	ΔS(kJ molH_2^{-1} K^{-1})	Source
Pd-$Pd_{0.6}$	8.2	0.77	0.72	−41.0	−0.0976	[7]
Mg-MgH_2	1×10^{-3}	2.0	7.66	−74.5	−0.135	[8]
Ti-TiH_2	4×10^{-17}	1.97	3.98	−164	−0.179	[9]

Table 1.1: Thermodynamic quantities for hydride formation at room temperature of palladium, magnesium and titanium.

1.1.3 Hydride formation

The hydrogen solubility limit is the maximum amount of hydrogen which can be absorbed inside a metal before a phase transition occurs. In a certain range of temperature and pressure, after reaching the solubility limit at concentration c_α, the absorption of more hydrogen in a metal M will have as a consequence the formation of a hydride phase with higher hydrogen concentration c_β. The absorption of hydrogen gas and phase separation can be written as [4]:

$$\frac{1}{c_\beta - c_\alpha}\mathrm{MH}_{c_\alpha} + \frac{1}{2}\mathrm{H}_2 \rightarrow \frac{1}{c_\beta - c_\alpha}\mathrm{MH}_{c_\beta} \tag{1.2}$$

The difference $c_\beta - c_\alpha$ corresponds to the width of the miscibility gap between the two phases. The term "hydride" does not always imply a change in the crystal structure. For the Pd-H system for instance, the fcc structure remains, just with a different lattice parameter. That is why sometimes these two regions are called α and α' phases. Table 1.1 shows some data for palladium, magnesium and titanium hydride formation.

1.1.4 Phase diagrams

Figure 1.3 from [10] shows the phase diagram of the binary system Pd-H at 1 bar of air pressure. At room temperature the hydrogen solubility limit is very small, around 0.01 H/Pd. Up to this concentration, only the so called α phase is present, the lattice parameter of which increases linearly with hydrogen concentration. For concentrations higher than that, the α' phase shows, having hydrogen content of about 0.60 H/Pd, with proportion to the α phase which follows the lever rule. When the α' phase is the only one present, adding more hydrogen results in a homogeneous increase of the hydrogen content all over the material.

The Mg-H phase diagram [11] shown in Figure 1.4 shows that up to a certain temperature the hydrogen reacts with the magnesium and forms MgH_2, with stoichiometric ratio H/Mg= 2, which corresponds to a hydrogen molar fraction $X_\mathrm{H} = 2/3$, as shown in the figure. MgH_2 shows a completely different structure (Figure 1.5) than crystalline Mg. The crystal structure of the latter in normal conditions is hcp. Magnesium hydride shows a rutile structure, which is based on a tetragonal unit cell.

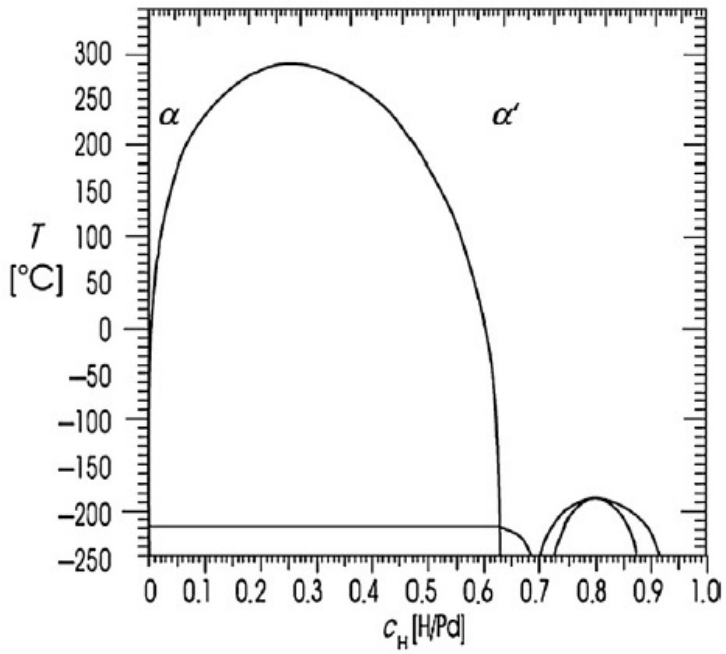

Figure 1.3: Phase diagram of the binary system palladium/hydrogen at standard ambient air pressure. At room temperature the solubility of hydrogen is very small, around 1 H atom every 100 Pd atoms. When this limit is reached, the α' phase starts forming. Above 293°C, the phase separation disappears and the hydrogen intake is homogeneous. This diagram is referred to a bulk-like volume of palladium. From [10].

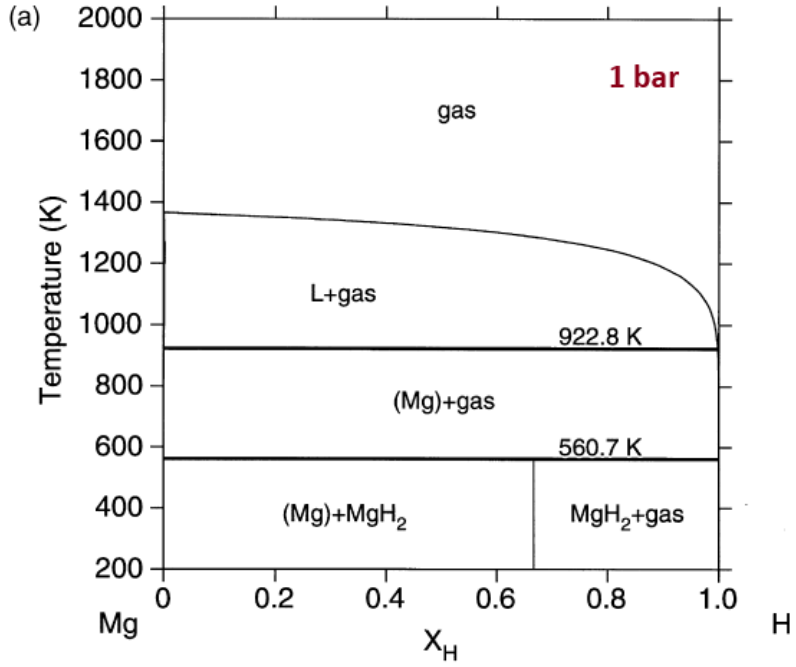

Figure 1.4: Phase diagram of the Mg-H binary system. The maximum hydrogen solubility in magnesium is very low: about $X_{\mathrm{H}} = 7 \times 10^{-4}$, right below the fusion temperature. The molar fraction of the hydride is $X_{\mathrm{H}} = 2/3$, shown by the vertical line at the bottom. Above 560.7K, no compound is forming. From [11].

The Ti-H system at atmospheric pressure appears to be more complicated than the one of Mg-H. Figure 1.6 shows that before reaching the stoichiometric compound, denoted as ε-TiH_2, the titanium can form other compounds, as the stoichiometric TiH and the so called δ-TiH_2, which has a hydrogen content which is slightly less than 2. All these phase changes happen at very low equilibrium pressure (See Table 1.1).

1.2 Hydrogen in thin films

1.2.1 Nano-size effects on equilibrium pressure

The metals used for this study are in the form of thin films. Thin films are structures restricted to the nanoscale in one spatial direction. Unlike bulk materials, these structures need to be deposited or grown onto a substrate which makes them stable. The presence of such substrate cannot be ignored.

The following is a model proposed by Mooij et al.[15] to explain the difference in the equilibrium pressure of magnesium thin films from magnesium bulk. In a few nanometers

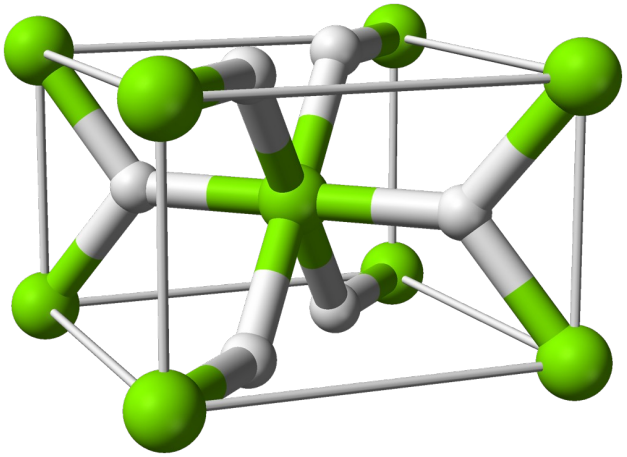

Figure 1.5: Rutile structure of MgH_2. It is based on a tetragonal structure. Green balls represent magnesium atoms, white balls represent hydrogen atoms. Image from [12]. Lattice parameters are $a = b = 4.48$Å and $c = 2.99$Å. It is an insulator with bandgap $E_g = 3.71$eV. Data retrieved from the Materials Project for MgH2 (mp-23710) from database version v2022.10.28.

thin film of magnesium, the hydride is assumed to be growing in discs, like in Figure 1.7. As the the magnesium hydride nuclei grow, the thin film expands only in the direction perpendicular to the substrate. This means that the surface area per mole of magnesium, which we call A, is the same for the two phases. Thus, the different energy of formation depends on the difference in interface energy density $\Delta\gamma$:

$$\ln\left(\frac{p_{\text{nano}}}{p_{\text{bulk}}}\right) = \frac{A}{RT}\Delta\gamma \tag{1.3}$$

Neglecting the small area of the Mg-MgH_2 interface and considering only top and bottom interface, we can write

$$A = \frac{2V}{d} \tag{1.4}$$

where V is the molar volume of magnesium and d is the layer thickness. This leads to an expression for the plateau pressure of a magnesium thin film with thickness d:

$$\ln\left(\frac{p_{\text{nano}}}{p_{\text{bulk}}}\right) = \frac{2V}{RTd}\Delta\gamma \tag{1.5}$$

From the experimental data Mooij et al. were able to determine $\Delta\gamma$ to be positive, meaning that for Mg-Ti multi-layers, thinner films have higher equilibrium pressure.

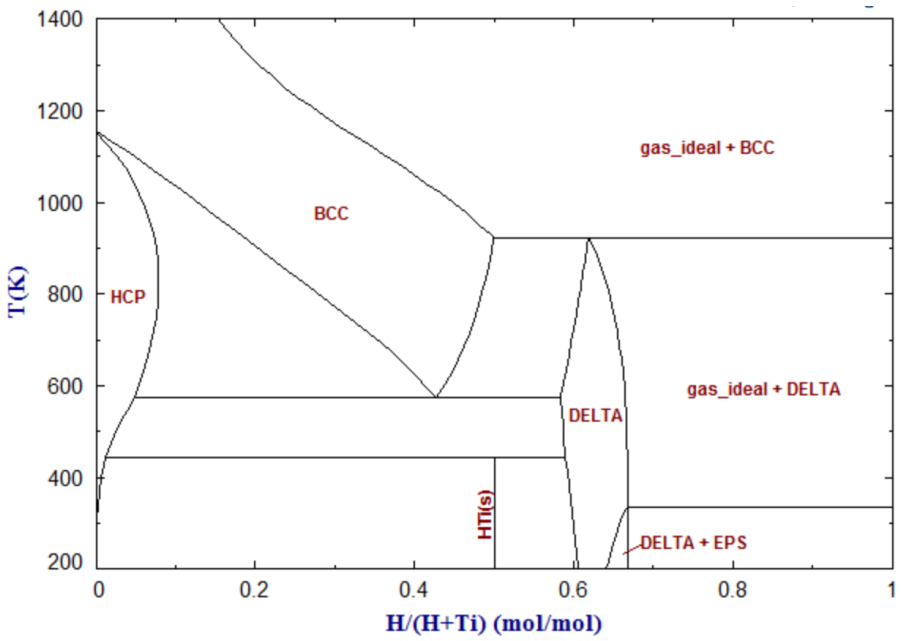

Figure 1.6: Phase diagram of the Ti-H system. Like for magnesium, the hydrogen solubility limit at room temperature is very small. Before reaching hydrogen saturation with TiH_2 a non stoichiometric compound called δ phase is formed, with hydrogen content slightly less than 2. Above 580°C, three phases with different hydrogen content can be formed: α (hcp), β (bcc) and δ (fcc). From FactSage database [13]. Data by [14].

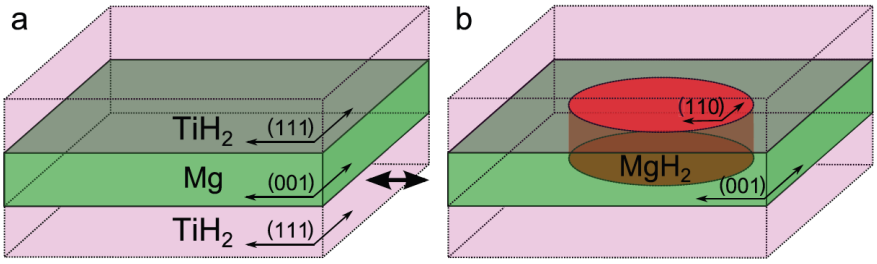

Figure 1.7: Magnesium hydride formation in a magnesium thin film. The hydride grows in discs. The surface between green and red region can be neglected as it is small compared to the cylinder faces. The film expands only in the vertical direction upon hydrogen intake. From [15].

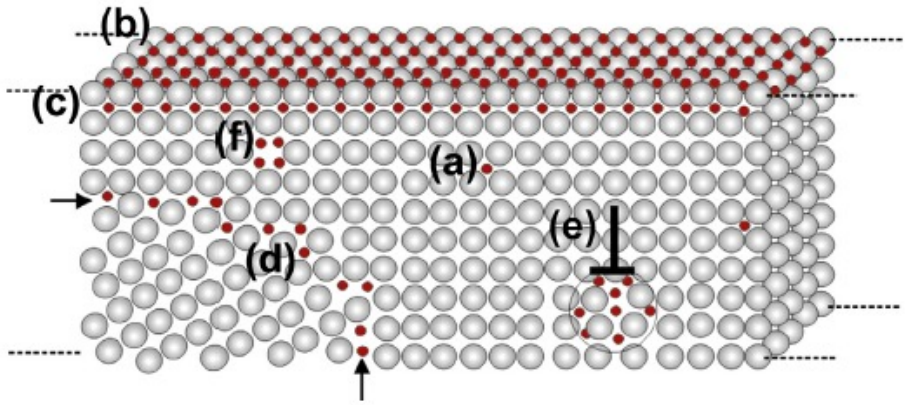

Figure 1.8: Illustration of the possible sites for hydrogen absorption in a metal: a) interstices; b) surface adsorption; c) subsurface adsorption; d) grain boundaries; e) dislocations; f) vacancies. From [18].

Another useful thermodynamic model is the one proposed by Wagner and Pundt for the Pd-H system [16]. In this model, the chemical potential of hydrogen in the palladium is a sum of the following terms:

$$\mu_{\mathrm{H}} = RT \ln\left(\frac{X_{\mathrm{H}}}{r - X_{\mathrm{H}}}\right) + E_0 - E_{\mathrm{HH}} X_{\mathrm{H}} - 2V\alpha_{\mathrm{H}}\sigma\left(X_{\mathrm{H}}\right) \tag{1.6}$$

The first term is the configurational entropy, where r is the maximum fraction of sites that can be occupied, which is left as a parameter. The second is a constant term accounting for the energy of the absorption sites, which for a standard palladium bulk are mostly interstices. The third is the energy of interaction between hydrogen atoms, which increases linearly with the hydrogen molar fraction X_{H}. The fourth term accounts for the change in the chemical potential caused by the in-plane stress $\sigma(X_{\mathrm{H}})$, where V is the molar volume of palladium and $\alpha_{\mathrm{H}} = 0.063$ is the expansion factor. As noted by Wagner, in case of linear elastic stress increase $\sigma = kX_{\mathrm{H}}$, with constant $k < 0$, the third and fourth term can be grouped and interpreted as a reduced E_{HH}. The reduced interaction between hydrogen atoms translates to a higher equilibrium chemical potential during phase transition and a lower miscibility gap. This is what is experimentally observed in bulk Pd samples with nano-sized grains [17].

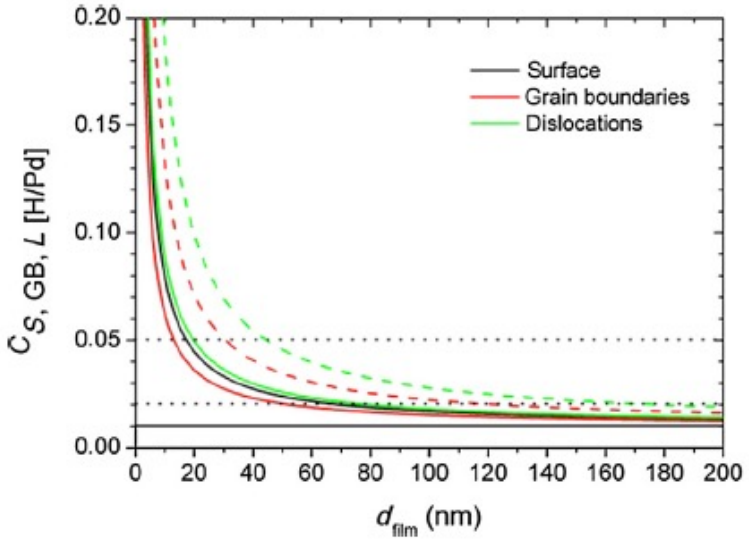

Figure 1.9: Hydrogen solubility limit in palladium depending on the film thickness. The horizontal black line indicates the bulk limit $c_0 = 0.01$ H/Pd. The red dashed line takes into account the contribution of surface and grain boundaries absorption and models a nanocrystalline film. The green dashed line takes into account the surface and dislocations, modelling an epitaxial film. For a 30 nm nanocrystalline thin film of palladium the solubility limit is increased of about 5 times with respect to the bulk. From [4].

1.2.2 Microstructure contribution to H solubility

Thin film usually contain a large volume fraction of defects. Also, the surface-to-volume ratio increases as the thickness decreases. Being hydrogen a very small atom, all these effects offer low energy sites where hydrogen can be initially trapped. This effect can be seen at low concentrations, where the chemical potential is lower than the one calculated using (1.6), assuming a constant E_0 for all concentration values. Figure 1.8 illustrates how hydrogen atoms can occupy the defects in a metal. Of all possible defects, vacancies are usually the ones which contribute less and will not be discussed in this study. Including surface and subsurface contributions the solubility limit c_α increases and becomes

$$c_{\alpha,S} = \frac{(d - d_s)}{d} c_0 + \frac{d_s}{d} c_s \tag{1.7}$$

where c_0 is the solubility limit of the bulk, d_s is the thickness of surface and subsurface and c_s its mean coverage. For example, it has been estimated that for palladium $d_s = 0.7$ nm and $c_s = 1$ H/Pd at room temperature [19]. If one instead considers the contribution of grain boundaries, the solubility limit changes like

$$c_{\alpha,GB} = \frac{(d - d_{GB})^2}{d^2} c_0 + \frac{2 d_{GB} d}{d^2} c_{GB} \tag{1.8}$$

where the grain size has been assumed to be equal to the film thickness. The concentration c_{GB} can be approximated as the average of the two phases. It is approximated like this, because this returns reasonable values. For palladium, it would be $c_{GB} = 0.3$. The grain boundary width for palladium was suggested to be $d_{GB} = 0.9$ nm [20].

The inclusion of surface and grain boundaries can approximate quite well the microstructure of a nanocrystalline film [4]. The effect of nanoscaling on the solubility limit of palladium is shown in Figure 1.9. For example, the solubility limit can go from a value of $c_0 = 0.01$ H/Pd in the bulk to $c = 0.05$ H/Pd for a 30 nm thick nanocrystalline thin film (red dashed line).

1.2.3 Effects related to stress

Thin film have a large surface-to-volume ratio which makes them unstable. In order to maintain their large surface they need to be deposited on a hard substrate, also called a stabilizer. The presence of such stabilizer means the thin film is unable to expand freely in all directions upon hydrogen absorption, but often just in the direction perpendicular to the substrate. This constraint result in high stress forces acting on the film in the directions parallel to the plane during hydrogen absorption. Figure 1.10 shows measured stress for different metals upon hydrogen intake. Stress increases linearly with the volume expansion according to the theory of linear elasticity [22], until it is released by formation of dislocations or film detachment.

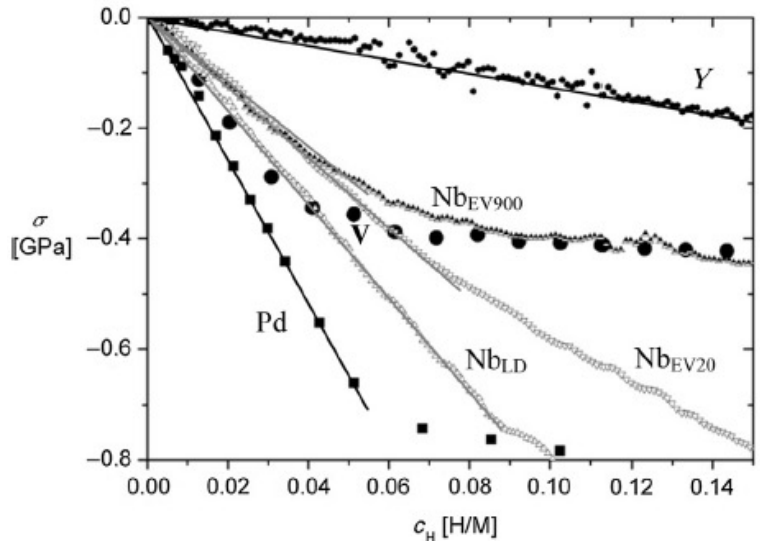

Figure 1.10: Measured stress induced by hydrogen intake for different 200 nm thick thin films. Initially the stress increase is linear, confirming linear elastic behaviour of the films. At higher concentration, stress increases more slowly due to formation of defects. From [4].

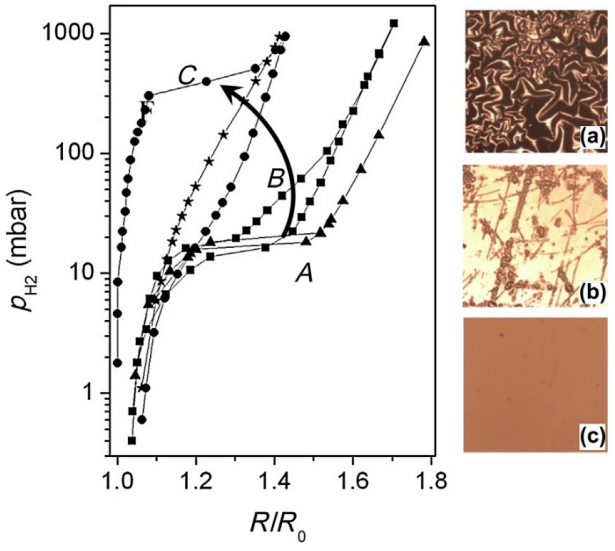

Figure 1.11: Effect of stress on equilibrium pressure of 200 nm thick Pd films, measured by increase in sample resistivity. (A) is a highly delaminated film, (B) is a partly detached film and (C) is a strongly bond film. From [21].

Figure 1.11 shows the result of stress forces on the isotherm curves, which measure change in equilibrium gas pressure upon hydrogen intake at constant temperature. If the film remains strongly bonded to the substrate, the high stresses translate to a higher equilibrium pressure of the phase change, as discussed in Section 1.2.1. As proposed by Wagner and Pundt [16], it can happen that before reaching the higher value of equilibrium, the stress becomes non-linear. This results in the observation of a plateau with a slope during hydrogen loading of thin films.

Chapter 2

Experimental methods

2.1 Sample fabrication

2.1.1 Sputter deposition

The technique used to fabricate the thin films is sputter deposition. It is a type of physical vapour deposition (PVD). It exploits the phenomenon of sputtering, which consists in particles being ejected from a target material when bombarded by energetic particles, in our case Ar^+ ions. The ejected particles condensate on a substrate, forming the thin film. The speed at which the thin film grows is called deposition rate and depends also on the target material chosen.

The machine used to fabricate the samples of this study is divided in two main parts: the chamber and the pre-chamber, separated by a manual valve. The chamber is mostly kept in Ultra High Vacuum (UHV) conditions, with a pressure of about 10^{-10} mbar. For the sputtering process, a flow of argon gas at a pressure of about 10^{-4} mbar is let into the chamber. Plasma is created in a separate RF source and then focused on the target. A rotating holder allows to choose among four different targets during deposition: palladium, magnesium, titanium and niobium. For this study only the first three were used. For magnesium and titanium, erosion of the target before deposition is necessary to remove oxide layers that may have formed on the materials surface, even at a background pressure of 10^{-10} mbar.

The pre-chamber is kept in high vacuum conditions, at about 10^{-7} mbar. When the sample holder has to be inserted, the vacuum pump is turned off and the pipe to the pre-chamber is closed with a valve. Then a flow of nitrogen gas is let in the pre-chamber, increasing the pressure, so the lid can be opened. This flow also prevents a large number of impurities from entering the pre-chamber. When the sample holder has been inserted, the vacuum pump is turned back on until the pressure is again 10^{-7} mbar. At that point, the valve between the two chambers is opened and the sample holder can be transferred to the main chamber for the deposition.

2.1.2 Types of samples

The main study was carried out on four types of samples:

- 30 nm thin film of palladium.
- 30 nm thin film of magnesium capped with a 30 nm thin film of palladium.
- A multi-layered structure made of two titanium layers and one magnesium layer in between, 5 nm each, capped with a 30 nm layer of palladium (5 nm Ti/5 nm Mg/5 nm Ti/30 nm Pd), for an expected total thickness of 45 nm. This type of sample is later referred to as type A.
- A multi-layered structure made of eight titanium layers and seven magnesium layers in between them, for a total of fifteen layers, capped with a 30 nm palladium layer ((1 nm Ti/1 nm Mg)×7/1 nm Ti/30 nm Pd), for an expected total thickness of 45 nm. This type of sample is later referred to as type B.

All types of sample are built on top of a 0.5 millimeters substrate of alumina (Al_2O_3), 1cm×1cm in size.

2.1.3 EDS

Energy Dispersive x-ray Spectroscopy (EDS) is a technique used to analyse the composition of a specimen. High energy electrons are sent onto the material and stimulate the emission of x-rays from the atoms present in the sample. The spectrum of the x-rays allows to identify the main elements in the specimen.

In this study EDS was used to study a sample of palladium, to make sure it did not contain a significant amount of impurities that would have made the measures ineffective. The sample is made of a 100 nm thin film of palladium deposited onto a 0.5 mm thick substrate of alumina (Al_2O_3). Since alumina is an insulator, the palladium film needs to be grounded using silver paste, in order to avoid charge accumulation during the electron scanning.

2.1.4 XRR

X-Ray Reflectivity (XRR) is a technique used to study surfaces and thin films. It exploits the interference of x-rays reflected by a sample to measure the thickness of the layers present on its surface. For example, it is the technique used to determine the deposition rate of different metals in the sputtering system described in Section 2.1.1. In this study we used the XRR to determine the thickness of the bi-layer in a sample of type B (See

Section 2.1.2), also called the super-lattice constant. Knowing the position of the more intense peaks, we can use Bragg's formula to determine the bi-layer thickness Λ [2]:

$$2\Lambda \sin\theta = n\lambda_{\mathrm{Cu}_{K\alpha}} \tag{2.1}$$

where n is the order of the diffraction peak.

2.2 Electrochemical hydrogen loading

2.2.1 Nernst equation

Let's consider the following reduction, happening at the surface of an electrode immersed in a solution:

$$2\mathrm{H}^+ + 2e^- \rightarrow \mathrm{H}_2(g) \tag{2.2}$$

From theory[23], the change in the Gibbs free energy is given by:

$$\Delta G = \Delta G^\circ + RT \ln Q \tag{2.3}$$

where ΔG° is the change in Gibbs free energy at standard state and Q is the reaction quotient.

The electrode voltage measures the tendency of the reaction (2.2) to take place. A positive voltage means the reaction tends towards the products, a negative voltage means it tends towards the reactants. Therefore, electrode voltage V and Gibbs free energy are two quantities that yield the same information, and share the following simple relation:

$$\Delta G = -nFV \tag{2.4}$$

where n is the quantity of electrons involved in the reaction. Comparing (2.3) and (2.4) leads to Nernst equation:

$$V = V^\circ - \frac{RT}{nF} \ln Q \tag{2.5}$$

The reaction quotient Q depends on the ratio between the activities of products and reactants. If the chemical species are sufficiently diluted, the activities coincide with the concentrations and the Nernst equation of reaction (2.2) becomes:

$$V = V^\circ + \frac{RT}{2F} \ln\left(\frac{[\mathrm{H}^+]^2}{p_{\mathrm{H}_2}}\right) \tag{2.6}$$

2.2.2 Metal-liquid system

Let's consider an electrode of palladium immersed in a solution containing H_3O^+ ions, which for simplicity we will consider as H^+ ions. If the concentration of H^+ ions is high enough, the reaction written in (2.2) will happen until equilibrium between ion concentration and hydrogen pressure is reached.

If the metal absorbs hydrogen, like palladium, another reaction happens, which is:

$$H^+ + e^- \rightarrow H_{Me} \tag{2.7}$$

where H_{Me} is the hydrogen that instead of forming hydrogen gas on the surface has been absorbed into the metal. Of course, absorbed hydrogen can diffuse back to the surface and leave the sample in the form of hydrogen gas, or in the form of H^+ ions, reversing (2.7). Therefore, the electrode potential will be determined by the hydrogen concentration near the surface of the metal. Electrochemical loading is a technique to study hydrogen concentration starting from this concept, and it is our technique of choice to produce and study metal hydrides. Moreover, it has several advantages with respect to other techniques, e.g. gas loading, given its simple procedure and flexibility to experimental conditions [24].

If a magnesium layer is present below the palladium layer, solutions with neutral or low pH cause the corrosion of the sample. This effect was seen when putting a palladium-magnesium sample in contact with a glycerol-phosphoric acid solution [25]. In order to avoid this, the electrolyte chosen for the cell is very alkaline. It consists of a 5 M solution of potassium hydroxide (KOH). KOH is a strong base that hydrolyzes almost completely in water. At the concentration of 5 M KOH, the pH of the solution is close to 14.7, which means the quantity of H^+ ions is less than 10^{-14} moles per liter. This means that, in order to cause considerable quantities of hydrogen to enter the sample, active water electrolysis is required. This can be achieved if the voltage difference between working and counter electrode (See Section 2.4) is high enough to cause the following reaction:

$$H_2O + e^- \rightarrow H_{Me} + OH^- \tag{2.8}$$

Reaction (2.8) is essentially equivalent to (2.7) and follows the same Nernst equation (2.6).

2.3 Hydrogen concentration

2.3.1 Charge method

The reaction (2.8) shows that each hydrogen atom that is formed on the surface needs exactly one electron, with a 1:1 ratio. Hence, if a constant current I passes through the

circuit for a time Δt the quantity of hydrogen that has formed on the metal will be [4]:

$$n_{\mathrm{H}} = \frac{I\Delta t}{F} \tag{2.9}$$

where F represents the charge of a mole of elementary charges $F = 96485\mathrm{C/mol}$ and is called the Faraday constant. If n_{Me} is the quantity of the metals in the sample which form the hydride, we can estimate the ratio hydrogen-to-metal atoms (H/Me) simply as:

$$\mathrm{H/Me} = \frac{n_{\mathrm{H}}}{n_{\mathrm{Me}}} \tag{2.10}$$

It is worth noticing that not all of the hydrogen formed enters the sample: given the small amount of metal, it is reasonable to expect that a considerable part of the absorbed hydrogen will stay close to the surface of palladium, as seen in Section 1.2.2. This effect is observable for current densities larger than 0.3 $\mathrm{mA/cm^2}$. On the surface atoms have the space to recombine and form diatomic hydrogen gas through the reaction

$$2\mathrm{H_{Me}} \rightarrow \mathrm{H_2} \tag{2.11}$$

If recombination is fast enough it can lead to the formation of hydrogen gas bubbles on the surface [26].

2.3.2 Transmittance variation method

An indirect way of measuring the hydrogen concentration in magnesium is to measure the transmittance of the film [15], which is proportional to, according to Beer-Lambert law:

$$n_{\mathrm{H}} \propto \log\left(\frac{T}{T_0}\right) \tag{2.12}$$

even if this relation does not account for the expansion of the thin film along the path of the light, which can modify the proportion. This method as used in our experiments does not provide a precise value of the ratio H/Me, but it can provide important information on when the majority of the transparent magnesium hydride is being formed. The combination of the transmittance and charge method together allows to have a more detailed description of the changes happening in the system.

2.4 The electrochemical cell

The frame of the cell is a 3D printed piece of plexiglass with a narrow space in which to pour the electrolyte and three holes to arrange the electrodes using the three electrode geometry:

- The sample is fixed face-down to the frame above a circular hole using screws. A rubber ring of 8 mm in diameter is put between the sample and the frame to act as a seal and preventing the electrolyte from spilling out. At the same time, a conducting wire is positioned under one of the corners sticking out of the ring in order to have electrical contact. This part of the cell is called the **working electrode** (WE).

- The **counter electrode** (CE) is a platinum foil immersed in the electrolyte and connected to a platinum wire which sticks out from a hole in the frame. The hole is sealed using glue.

- The **reference electrode** (RE) is based on a small glass capsule containing a Hg/HgO mixture immersed in a 1M KOH solution. It has a long glass tube at the end of which is a small ceramic fret, which has to be immersed in the electrolyte. It is a reference electrode suitable to be used in highly alkaline solutions.

As stated in Section 2.2.2, the electrolyte is a concentrated 5M KOH solution. The frame of the cell is made out of plastic instead of glass in order to avoid corrosion that happens due to long exposure to a strong base. Before using it, the electrolyte is bubbled for about thirty minutes with argon gas in order to remove the oxygen gas that could be present.

2.5 The complete circuit

Figure 2.1 shows the schematics of the circuit in the original configuration:

- A **SMU** (Source Measure Unit) provides a fixed voltage between WE and CE. The working electrode has to be set at the lower voltage for the reaction to happen.

- An **impedance converter** connected between RE and WE prevents the current from flowing through the reference electrode and returns the voltage between the two.

- A manually activated **relay** closes the circuit for the time chosen, usually 4 seconds.

- A 1 kΩ **resistor** is put in series with the cell. The voltage drop across the resistor is measured to determine the current flowing in the circuit.

- A **DAQ** samples the signals coming from the resistor and the impedance converter. The data is saved to the PC using the DAQ software.

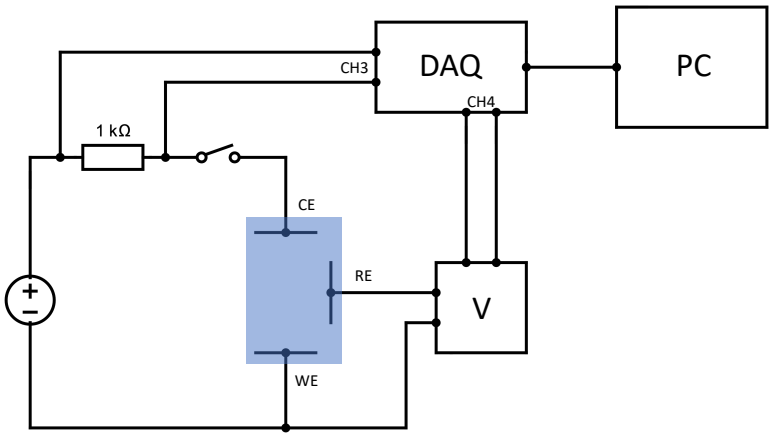

Figure 2.1: Schematics of the original circuit. The blue rectangle represents the electrochemical cell.

Separated from the electrical circuit is the experimental apparatus used to measure the sample transparency. It consists of an optical microscope with a light source directly below the sample. A CCD camera controlled by a software allows to take pictures of a small portion of the sample and save them as image files that can be analyzed later. The microscope and the cell were placed under a fume hood to prevent hazards from the use of the electrolyte.

2.6 Automation

2.6.1 SMU automation using TSP and Python

The experimental setup shown in Section 2.5 presents some limits such as:

- The relay has to be activated manually. This means less time precision between pulses, with a different number of samples per pulse, thus complicating the data analysis afterwards.
- Sourcing voltage means there is never a steady current flowing in the circuit. Since the resistance of the cell can easily vary the current is not constant through the pulse duration, thus making (2.9) invalid. This is not much of a problem, as in order to obtain the correct value for charge, one simply has to integrate the current over time.

One way to overcome these issues is using Keithley's built-in programming language called Test Script Processor (TSP) and a Python package called PyVISA. TSP can be

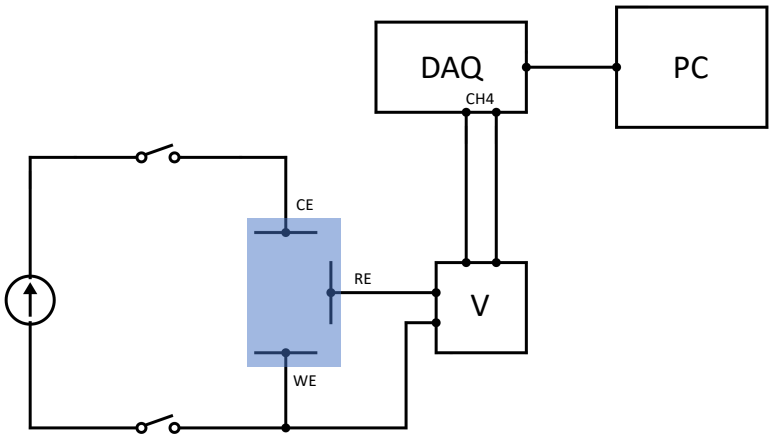

Figure 2.2: Schematics of the new circuit. The voltage source is changed to a current source. The two switches that close the circuit for the set time are digitally controlled by the Arduino.

seen as an equivalent of SCPI (Standard Commands for Programmable Instrumentation). The latter is not supported on the series of our Keithley instrument. PyVISA is a wrapper for the standard way of configuring and programming instrumentation systems called VISA (Virtual Instrument Software Architecture). Using the combination of these two languages, one can write a simple script that programs the SMU in current mode and set the current at the desired values for a precise amount of time. See Appendix A for the code details.

2.6.2 Digital relay using Arduino

Another way to automatize the procedure is to use a programmable Arduino as a digital relay. Using the SMU in current source mode and the Arduino relays the circuit diagram becomes as the one in Figure 2.2. This was the final configuration of choice as it is more similar to the manual one. A C++ script is used to program the Arduino to open/close the switches within a set time. See Appendix B for the code details. The Python scripts developed for the analysis in this thesis are shown in Appendix C.

Chapter 3

Results and discussion

3.1 EDS and XRR measurements

The result of the EDS measurement on a small portion of a 100 nm Pd layer deposited onto an Al_2O_3 substrate are summarized in Figure 3.1. Table 3.1 shows the quantity of elements resulting from the spectral analysis. The analysis shows a high content of carbon, oxygen, aluminum and palladium. Impurities like nickel and iron are present in very small amounts and are therefore negligible. The high content of carbon is probably due to the SEM imaging itself. Al and O are present in the substrate. This means that the sputtering system produces films of high quality and the samples can be from now on considered to be made of pure elements. Figure 3.2 shows the interference pattern of reflected x-rays as a function of the incident angle on a multi-layered sample of titanium and magnesium. In the figure, two prominent peaks appear due to the constructive interference given by the super-lattice. Using Bragg's formula shown in Section 2.1.4, we can calculate the super-lattice constant by the position of these peaks. For both peaks we obtain $\Lambda = 2.0$ nm, as expected for the sample Sapphire/(1nm Ti/ 1nm Mg)×7/1 nm Ti/30 nm Pd.

3.2 Hydrogen loading using manual relay

3.2.1 Pd thin film

Figure 3.3 shows the hydrogen loading of a 30 nm thin film of palladium using short pulses of current. According to (2.9) and (2.10), measures on current suggest that after each pulse the ratio H/Pd should be increasing of about 0.16, neglecting the hydrogen which is diffusing out of the metal. Therefore, already after the first pulse the system should be in the Pd-PdH_x phase transition region, according to the phase diagram of the Pd/H system and even if we account for increased solubility limit in the thin film,

Element	Weight %	Atomic %	Error %
C	39.9	66.3	11.0
O	7.7	9.6	11.9
Al	25.7	19.0	5.5
Fe	0.2	0.1	32.3
Ni	0.2	0.1	41.4
Pd	26.2	4.9	3.3

Table 3.1: Composition of the palladium sample resulting from the spectrum fitting shown in Figure 3.1. Iron and nickel impurities are present in small quantities. Aluminum and oxygen atoms are present in the substrate.

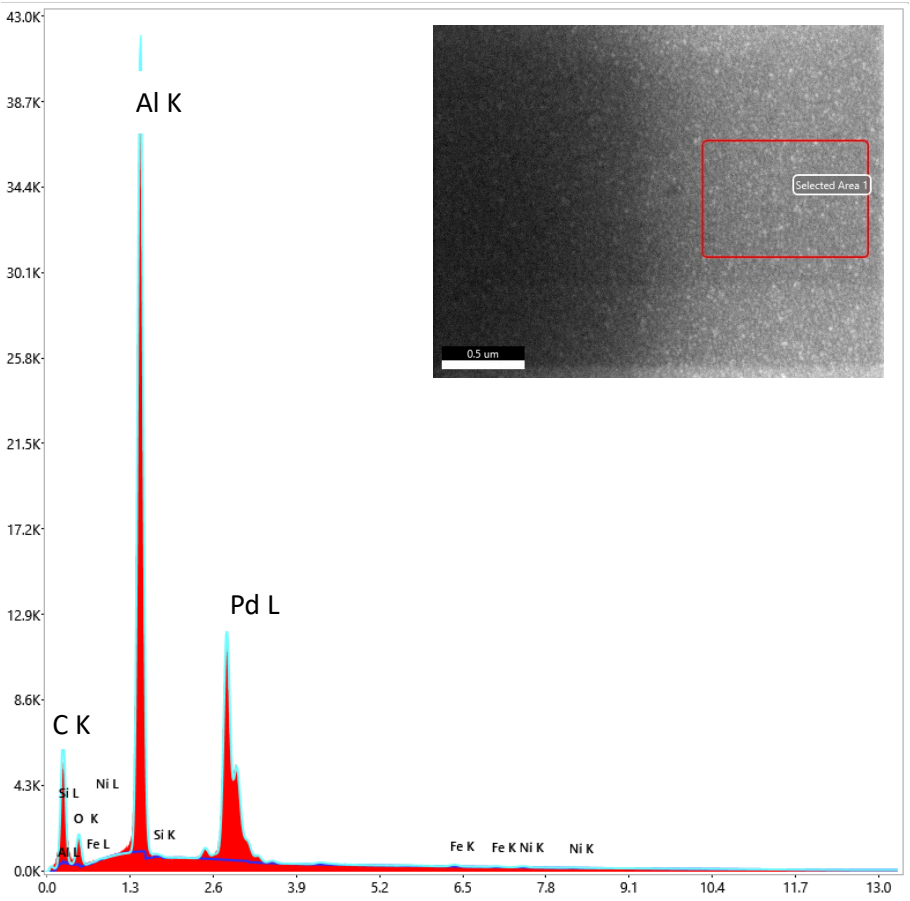

Figure 3.1: EDS measurement taken on a 100nm palladium thin film deposited on a Al_2O_3 substrate. The x-axis is in keV and the y-axis in photon counts. Measure performed by Dr. S. Schlabach, IAM-WK, and J. Wild, IAM-WK, at KIT Campus Nord.

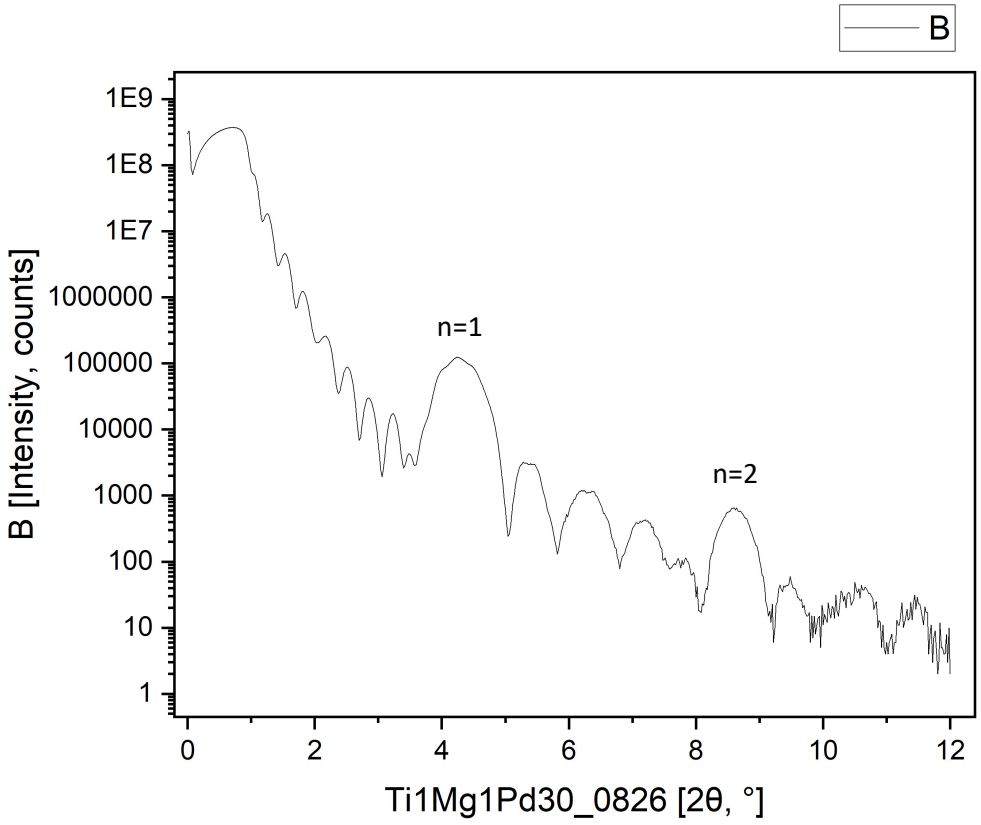

Figure 3.2: XRR measurement taken on a multi-layered sample of type B (See Section 2.1.2). Constructive interference of reflected x-rays at certain angles (highlighted in the figure with the index n) allows to determine the thickness of the Mg/Ti bi-layer. Measure performed by Dr. S. Wagner, IAM-WK, at KIT Campus Nord.

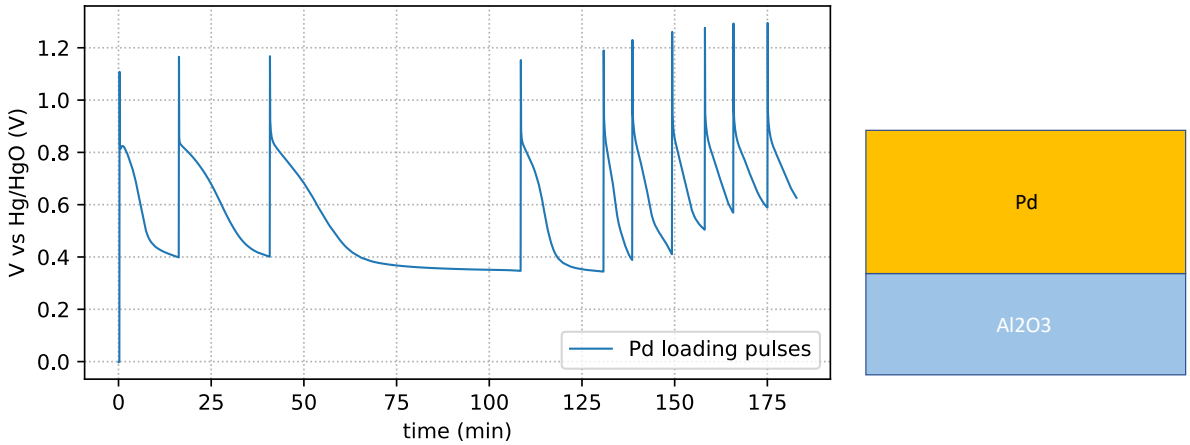

Figure 3.3: Hydrogen loading of a 30 nm thin film of palladium with different waiting times between each pulse. The vertical lines correspond to 4 s pulses. On the y-axis the absolute value of the voltage is measured.

as seen in Section 1.2.2. In fact, the voltage of the first pulse in Figure 3.3 looks like it is stabilizing around 400 mV. This is in agreement with previous works that used the same reference electrode and experimental setup [26] [25].

Other experimental findings concerning the measure in Figure 3.3 show up:

- An initial equilibrium at around 800 mV due to high hydrogen concentration on the surface is disturbing the measure.
- The curves at the equilibrium are never perfectly flat when the equilibrium voltage is reached, but always slowly decreasing.

The first effect could be due to additional reactions happening at the palladium surface. It might also be that the surface is polarized, and the surplus charge needs to be removed. This problem was mitigated in the following measures with the use of shorter pulses and lower currents. The second effect could be related to the loss of hydrogen from the thin film.

3.2.2 Mg/Pd thin film

Figure 3.4.a shows the hydrogen loading of a 30 nm thin film of magnesium capped with a 30 nm thin film of palladium. In this case the data are taken experimenting with different loading times, varying from 0.1 s to 4 s. The waiting time between each pulse is around three minutes. If we take the points at the end of the first four pulses, the value of the potential is increasing (actually decreasing, since we are measuring $-V$). This value is then stable for about twelve more peaks, at around 330 mV. It then rises a little bit at about 370 mV. At this point increasing the loading time causes the curve to descend more slowly. Taking the last voltage value in each curve produces the set of points in the y-axis of Figure 3.4.c and Figure 3.4.d. In the former the x-axis is the hydrogen concentration in the Mg layer, as it is supposed to load before the Pd layer. In the latter, the x-axis is the logarithm of the transmittance.

The points at constant voltage at 330 mV represent the concentration range in which magnesium hydride is being formed. This value is in agreement with previous works [26]. The Mg-MgH_2 transition region is shown in detail in Figure 3.4.b. In Figure 3.4.c one should expect the ratio H/Mg to be ≈ 2 when the equilibrium value rises. Instead, the calculated value is closer to H/Mg ≈ 1.5. A possible explanation is the formation of a Pd-Mg alloy at the interface. If we consider a pure Mg layer thickness of 25 nm instead of 30 nm, the resulting concentration is close to the expected value H/Mg = 2. Another possible reason is the change of experimental parameters during the measurement. Increasing the voltage and/or the loading time leads to more hydrogen accumulating on the sample surface with unwanted effects, as seen in the previous section. This change may have lead to an artificially raised equilibrium voltage. Since the H solubility in Mg is very small, according to Figure 1.4, already after the first pulse the phase change equilibrium voltage should be reached. But Figure 3.4 shows that it takes about four pulses of current to reach a plateau. This may be due to the increased solubility limit of palladium, which initially offers lower energy sites for the hydrogen to occupy, as discussed in Section 1.2.2. The first four pulses correspond to a hydrogen concentration in palladium of H/Pd ≈ 0.04, which is lower than the calculated solubility limit in a nanocrystalline 30 nm palladium thin film.

The analysis on the sample transmittance (Figure 3.4.d) confirms that indeed the formation of MgH_2 happens during the first plateau, corresponding to the largest increase in transparency. Figure 3.5 shows different picture of a small portion of the sample as seen from the optical microscope during various stages of the pulse loading. The circular pattern is likely due to the shape of the rubber ring which presses onto the sample.

3.2.3 Mg/Ti multi-layers

Figure 3.6.a shows the hydrogen pulse loading of a sample of type A (See Section 2.1.2). The pulses are given manually and have duration from 0.1 s to 1 s. The waiting time

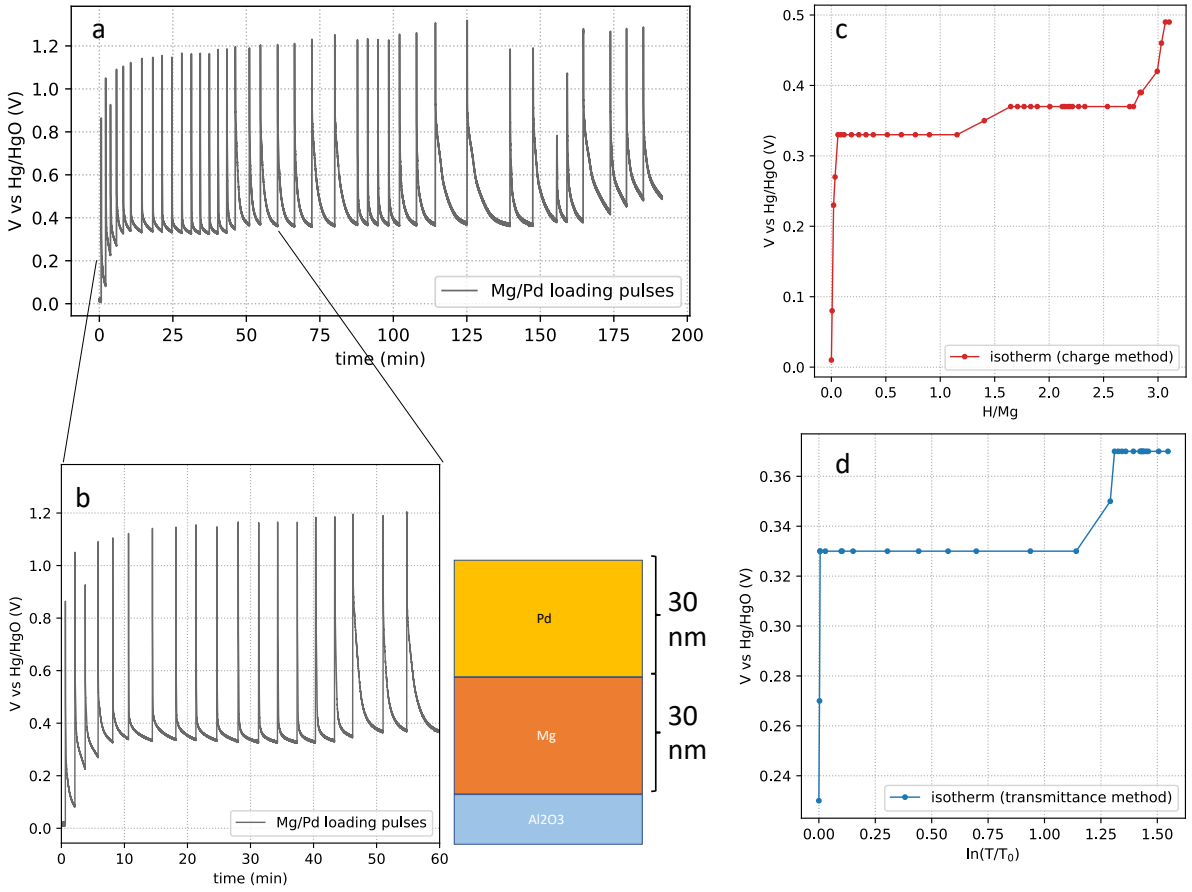

Figure 3.4: Electrochemical hydrogen loading of a 30 nm Mg thin film capped by a 30 nm Pd thin film. a) Working electrode voltage (absolute value) versus time. b) Detail of the region where magnesium hydride is formed. c) Isotherm with calculated composition using the charge method. d) Isotherm with measured transmittance.

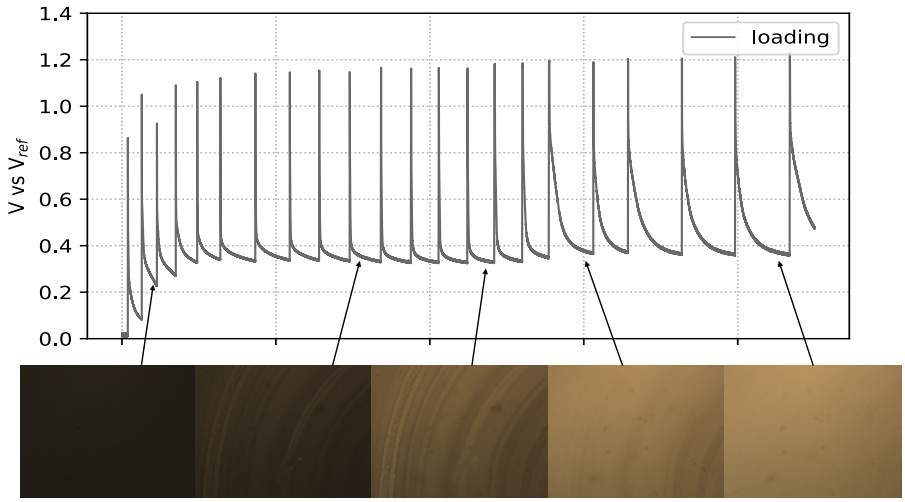

Figure 3.5: Magnesium hydride formation at different stages as seen from the optical microscope. The sample gets more and more transparent as the hydrogen concentration increases. The circular pattern is due to the circular shape of the o-ring which applies pressure on the thin film.

between pulses is around 3 minutes. Considering only the last point of each curve, the voltage appears to be constant at the beginning and then slowly rise after reaching a new constant value at 400 mV. Figure 3.6.b shows the set of voltage points versus the sample transmittance. An increase in transmittance is expected for when the MgH_2 is forming, in the metal-to-insulator transition. Since TiH_2 is non-transparent, the change in transmittance during its formation should be zero. Moreover, according to Section 1.1.3, titanium hydride should form before magnesium hydride. Figure 3.6.c shows the set of voltage points versus the calculated concentration of hydrogen in the Mg and Ti layers.

According to these results, the following sequence can be suggested: at the beginning, TiH_2 is forming, due to its lower energy of formation (Section 1.1.3). When the top layer of titanium hydride has completely formed, it is possible that the bottom layer of titanium acts as a hydrogen sink, slowly absorbing the hydrogen through the magnesium layer. When also the second layer of titanium hydride has formed, the layer of magnesium starts forming MgH_2. The analysis on transmittance in Figure 3.6.b shows that the largest increase in transparency is right before the plateau at 400 mV, which is when the hydrogen starts accumulating in the palladium, according to the results in the previous sections. This suggests that the magnesium layer loads after the titanium hydride has completely formed in the other two layers. It is possible that in this case the magnesium layer loads more slowly than the Mg/Pd thin film, due to the presence of the titanium hydride layer in between. The slower diffusion may be responsible for the

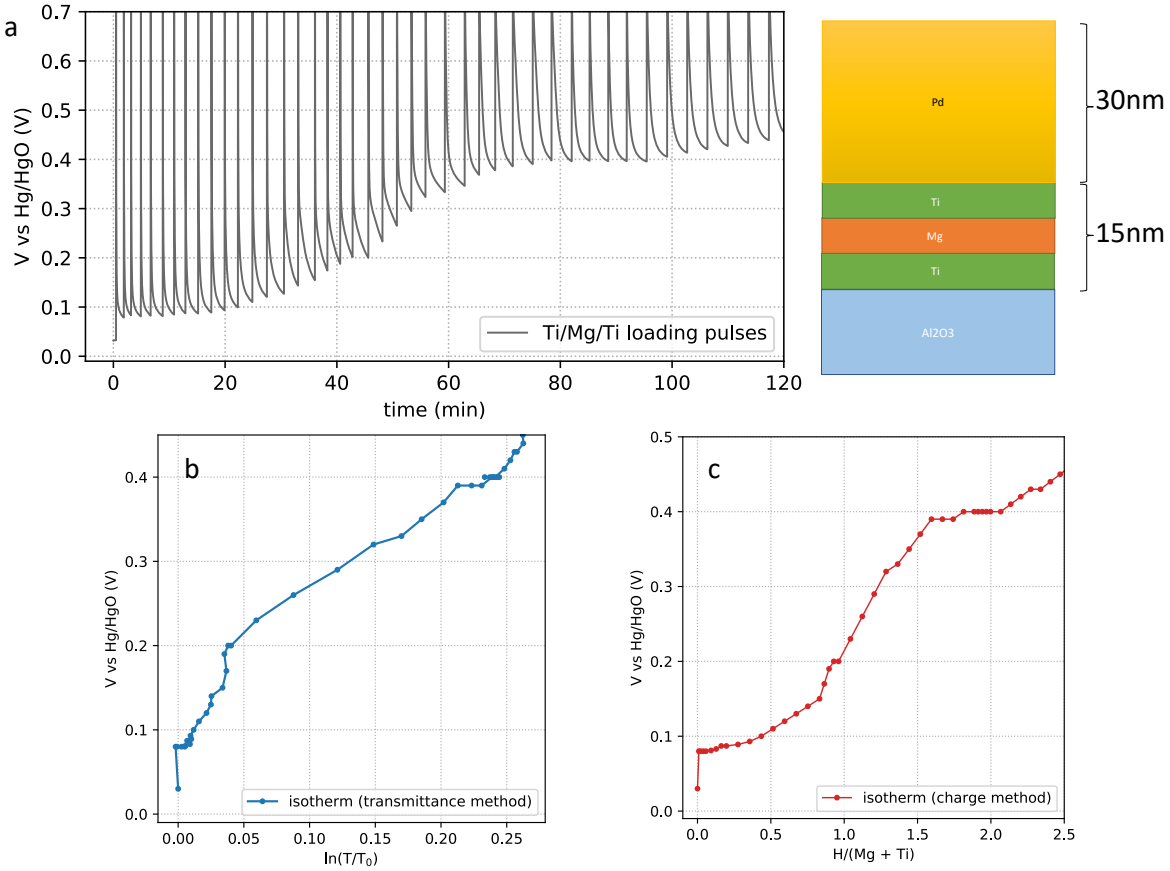

Figure 3.6: Electrochemical hydrogen loading of a multi-layered sample of type A (See Section 2.1.2). a) Absolute value of voltage versus time. b) Isotherm with measured transmittance increase. c) Isotherm with calculated hydrogen concentration using the charge method.

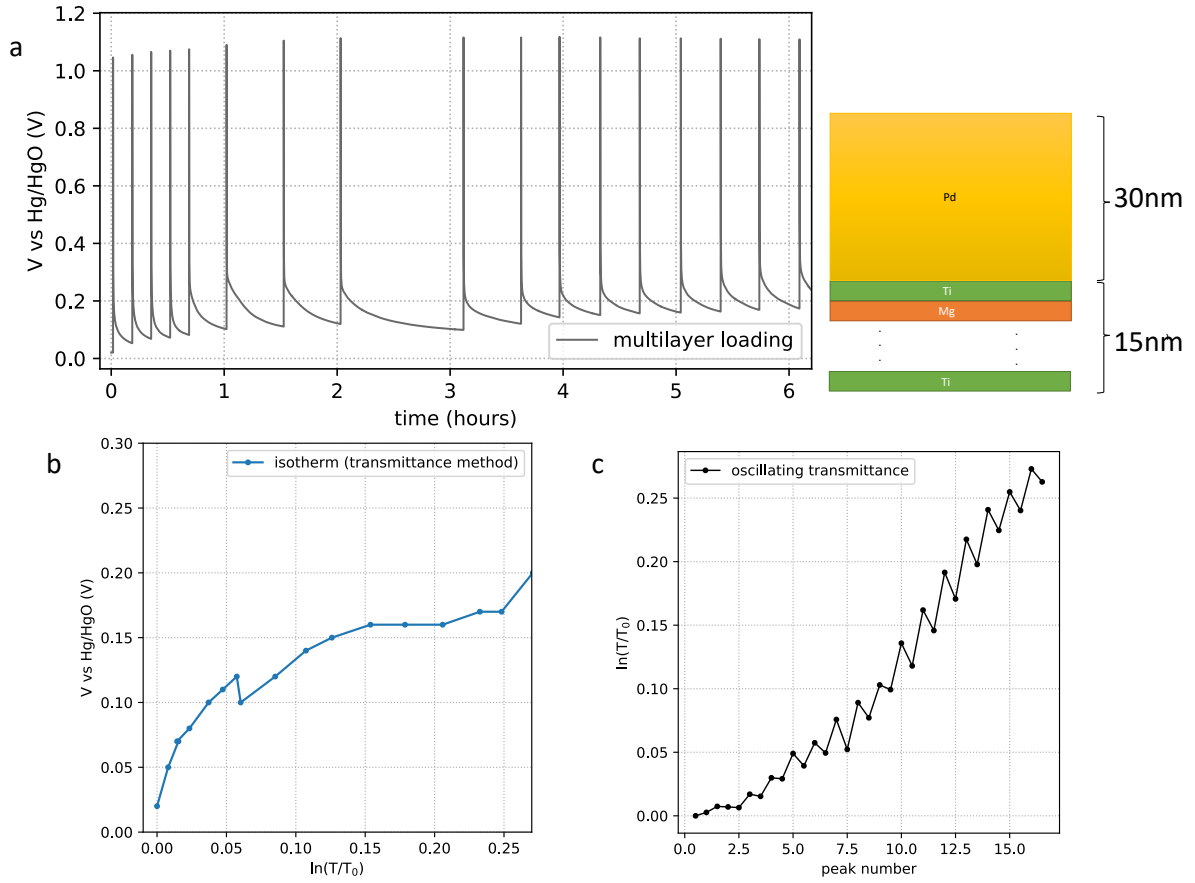

Figure 3.7: Electrochemical hydrogen loading of a multi-layered sample of type B (See section 2.1.2). a) Absolute voltage value versus time. b) Isotherm with measured transmittance. c) Oscillating transmittance with two pictures taken at the beginning and at the end of each pulse.

disappearance of the equilibrium plateau of magnesium hydride. Figure 3.6.c shows that at the beginning of the Pd/PdH_x equilibrium plateau to concentration in the bottom three layers is H/(Mg+Ti)$\approx$ 1.5.

Figure 3.7.a shows the hydrogen loading of a multi-layered sample of type B, which is made by a layers of titanium and magnesium alternated, for a total of fifteen layers (See Section 2.1.2). The pulse duration is fixed to 1 s. The waiting time between two pulses is long, varying from 10 minutes to 1 hour. Figure 3.7.b shows the last voltage value of each curve versus to the sample transmittance. Figure 3.7.c shows the value of transmittance of pictures taken at the beginning and at the end of each curve. The former are labeled with half-integer numbers and the latter with integers.

The almost regular transmittance increase in Figure 3.7.b suggests that new magnesium hydride is indeed formed after every step. In this case, diffusion is much slower than in other types of sample. This means a much longer time is needed after a pulse in order to reach the chemical equilibrium condition. In Figure 3.7.c, the sample transparency at the beginning of each curve is always higher than the transparency at the end. This result suggests that after each current pulses magnesium hydride is formed and then partially dissolved due to hydrogen diffusion in the titanium layers, given the higher stability of TiH_2.

3.3 Hydrogen loading using automatic relay

3.3.1 Mg/Ti multi-layers

The results shown in Section 3.2 suggest changes to the experimental parameters in order to have a better accuracy and understanding:

- The operator should be able to provide a stable current and not a stable voltage, in order to compute more easily the quantity of hydrogen entering the sample, using 2.9.
- The pulse duration should be short, e.g. less than 2 seconds, and the current small, e.g. less than 1 mA, in order to avoid unwanted effects. This is due to the small surface which is in contact with the electrolyte and the small quantity of metals present in the samples that can get saturated quickly.
- The waiting time between each pulse should be relatively short, e.g. less than ten minutes. Otherwise, the quantity of hydrogen diffusing out of the sample through 2.11 becomes not negligible.
- The waiting time between each pulse should be exactly the same. This makes it easier to elaborate the data. Also, the regularity of the pulses makes it possible to

take different curves corresponding to different timestamps during the relaxation. This can highlight diffusion effects that would be otherwise hidden.

To meet the first three conditions it is sufficient to change some parameters. In order to meet the last condition, it is necessary to modify the experimental apparatus and use a programmable relay, like an Arduino (see Section 2.6). Two measurements of this kind were carried out: one on a sample of type A, shown in Figure 3.8 and the other one on a sample of type B, shown in Figure 3.9. Both measurements were taken using 1 s pulses at 0.5 mA and waiting 5 minutes before the next pulse, for a total of 100 pulses. Figure 3.8.c and Figure 3.9.c show the isotherms with the calculated hydrogen concentration on the x axis, but this time the points chosen are more than one per pulse. The resulting curves show different behaviors depending on the time which they refer to after each pulse. This property can be exploited in order to gain more information about the diffusion inside the sample.

3.3.2 Plateau width

In Figure 3.8.c, two main regions in which the voltage is either almost flat or decreasing can be spotted. These regions happen to be between the same concentration values for all the curves in the figure. The first is approximately between the values 1.5 and 2 of hydrogen content. The second one is approximately between the values 2.5 and 4. In these regions the curves are further apart from each other. This suggests that those are the regions where the hydrogen diffusion inside the sample slows down. In the case of sample A, the first plateau corresponds to the TiH_2 being completely formed and the start of the formation of MgH_2. At the end of this plateau, if we compute the hydrogen content for all the points so far we obtain H/(Mg+Ti)= 2.1 ± 0.2. This is in accordance with the expected value of 2. If we consider only the points which form the plateau and substitute the quantity of Mg in the denominator, we obtain H/Mg= 2.0 ± 0.2, which is again in accordance with the stoichiometry of the reaction. If instead we consider only the points in the second plateau, and substitute the quantity of Pd in the denominator, we obtain H/Pd= 0.49 ± 0.05, which is the expected miscibility gap for a thin film of palladium.

Figure 3.9.c shows a more complicated picture for the sample of type B. The curves appear to be further apart from the beginning. Approximately between 1.5 and 2.5 hydrogen content, two smaller plateaus appear close to each other instead of a large one. Approximately between 4 and 5 H/(Mg+Ti), another plateau appears, recognizable as the plateau of palladium hydride formation. The fact that at the beginning the curves of different colors are further apart than in the previous case means the diffusion is slow from the start. This is reasonable since the layers are very thin, meaning the hydrogen has to pass through various magnesium layers before reaching empty titanium layers. As can be seen from the figure, at the end of the Mg plateau the hydrogen concentration is

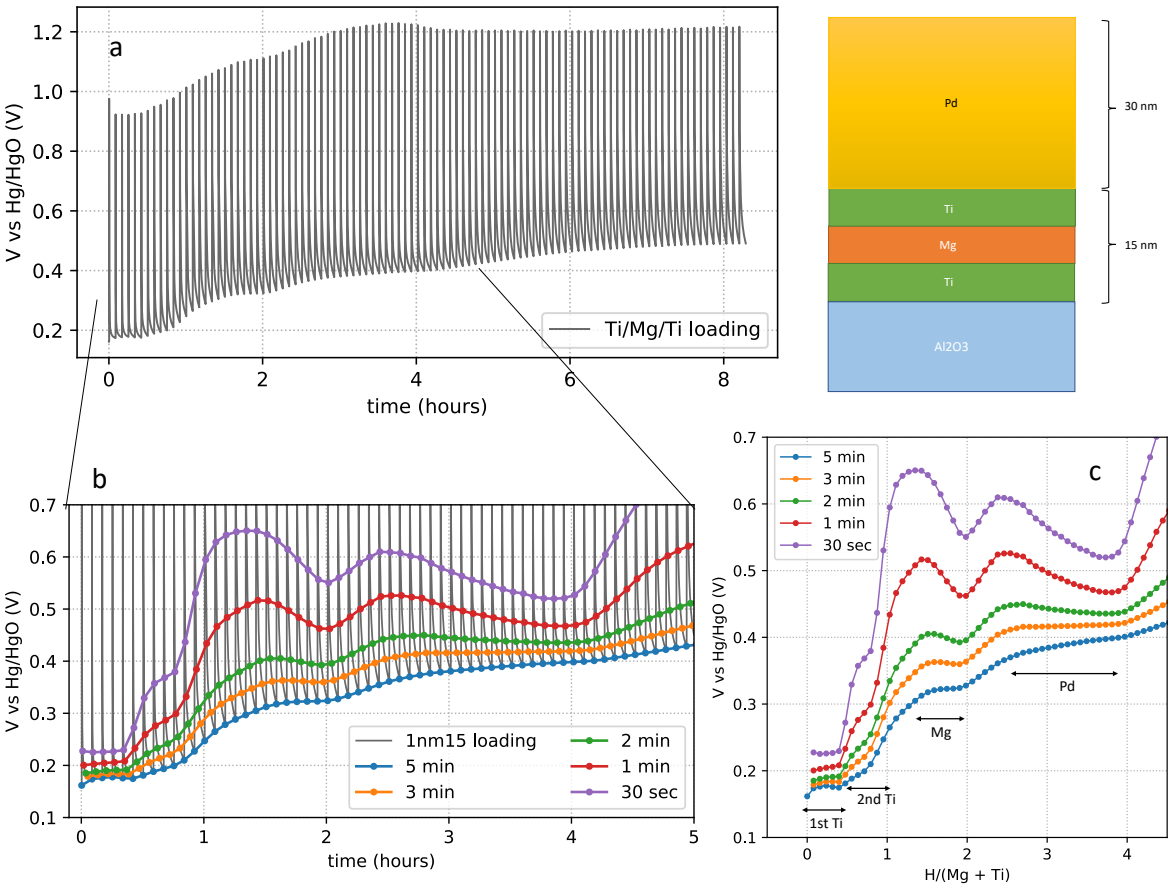

Figure 3.8: Electrochemical hydrogen loading of a sample of type A (See Section 2.1.2) with equal pulses. a) Absolute voltage value versus time. b) Voltage values taken with regular timing after the each pulse. c) Isotherm of the different voltages using calculated hydrogen content.

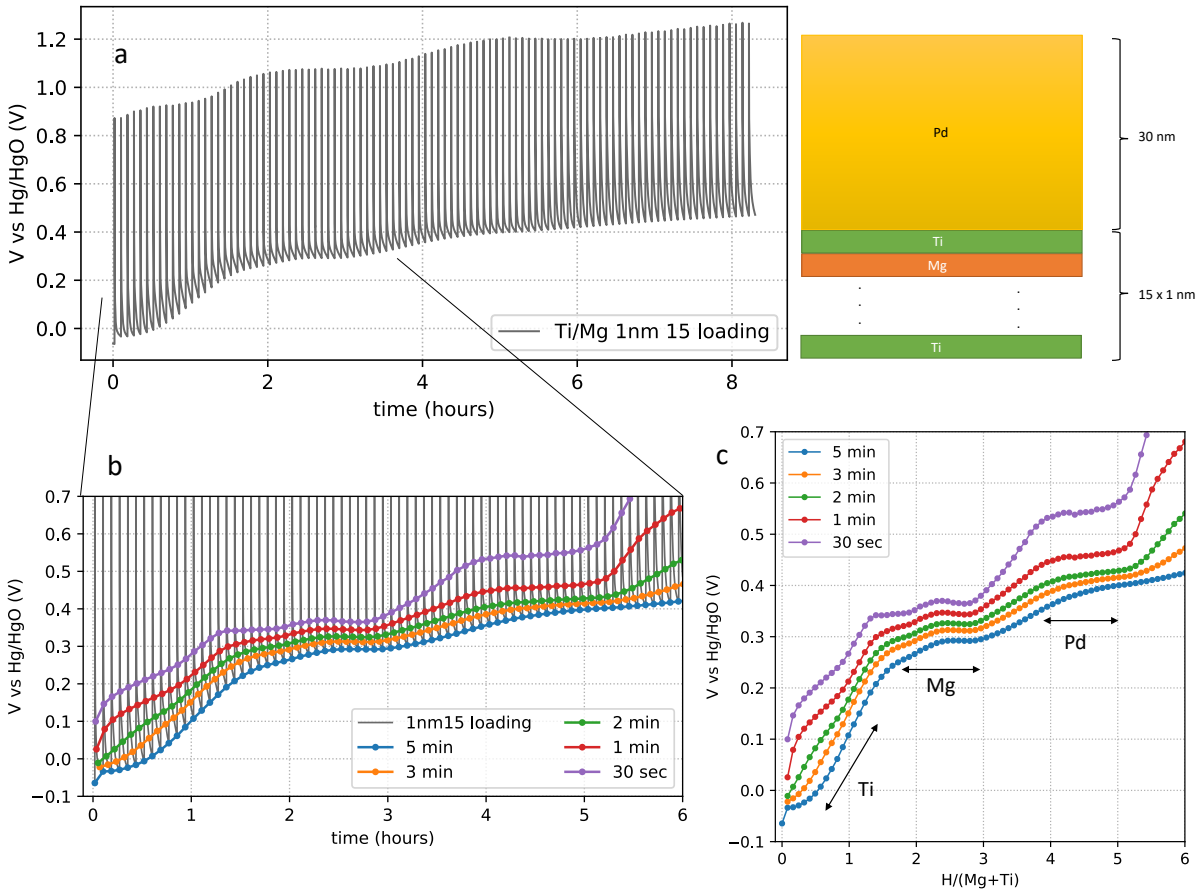

Figure 3.9: Electrochemical hydrogen loading of a sample of type B (See Section 2.1.2) with equal pulses. a) Absolute voltage value versus time. b) Voltage values taken with regular timing after the each pulse. c) Isotherm of the different voltages using calculated hydrogen content.

almost H/(Mg+Ti)= 3, a value which is not acceptable. Since this technique has revealed to be highly dependent on the internal diffusion mechanisms, it is no surprise that the sample with more complex layering returns unsatisfying results. A possible explanation may be that for this type of sample the time required to reach the equilibrium condition at some point may be longer than five minutes, thus complicating the data interpretation. More experiments should be made with this type of measure on samples having simpler structure, before a reliable quantitative analysis can be carried out for multilayers.

3.3.3 Equilibrium voltage level

One of the goals of this work was to determine the equilibrium voltage in multilayers with different thicknesses and number of layers using electrochemical pulsed loading. Since this technique has proven to be heavily dependent on the speed of diffusion inside the sample, the determination of a precise phase transition voltage for multilayers is quite difficult. More experiments should be carried out using longer waiting times.

3.3.4 Hydrogen out-diffusion

After loading the two samples even beyond the Pd/PdH equilibrium voltage, they are left in contact with the electrolyte until next day. This causes the potential to slowly decrease due to hydrogen out-diffusion in the form of hydrogen gas. Figure 3.10 shows the descending curves for both samples. As expected, out-diffusion is faster when hydrogen is present in higher concentration, which corresponds to the larger decrease in hydrogen chemical potential. The timescale at which the voltage decreases suggests that if the waiting time between pulses is short enough the quantity of hydrogen which leaves the sample can be neglected in the calculation of the hydrogen content. Though, this waiting time has to be long enough to allow the chemical potential to be equal everywhere in the sample. This may be a problem for samples with many layers, as sample B. Figure 3.11 shows the surface of sample B during three stages of the experiment. After six hours it can be seen that the sample is more transparent, as the magnesium hydride has formed. After twenty-four hours, the sample has returned to its original transparency after out-diffusion, and clear spots of oxide/hydroxide on the palladium surface have formed due to the long exposure to the electrolyte.

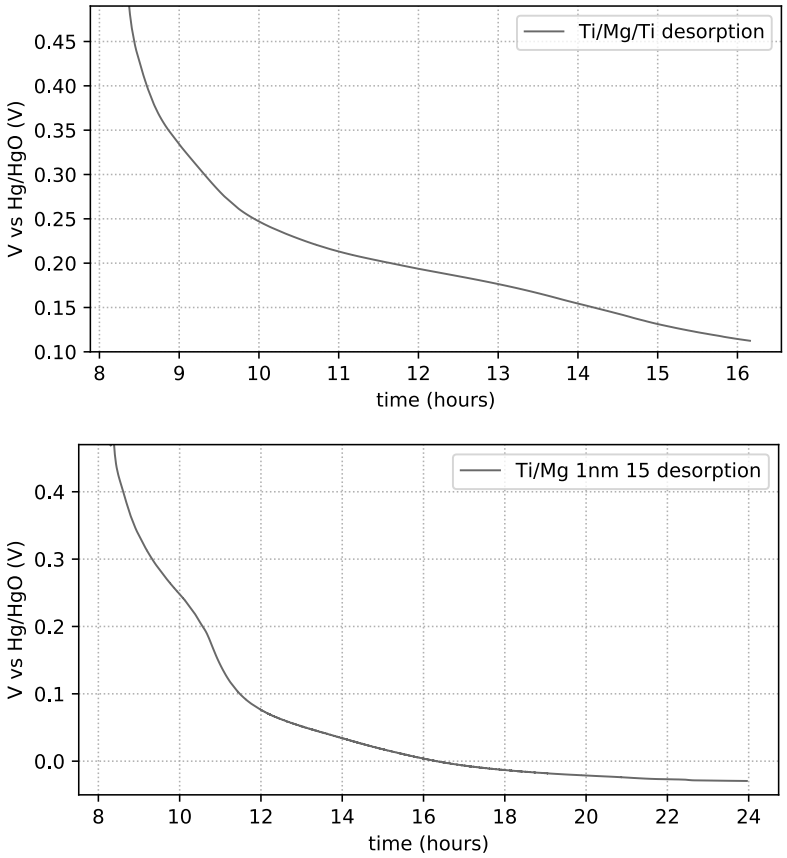

Figure 3.10: Hydrogen desorption. Top) Sample A. Bottom) Sample B.

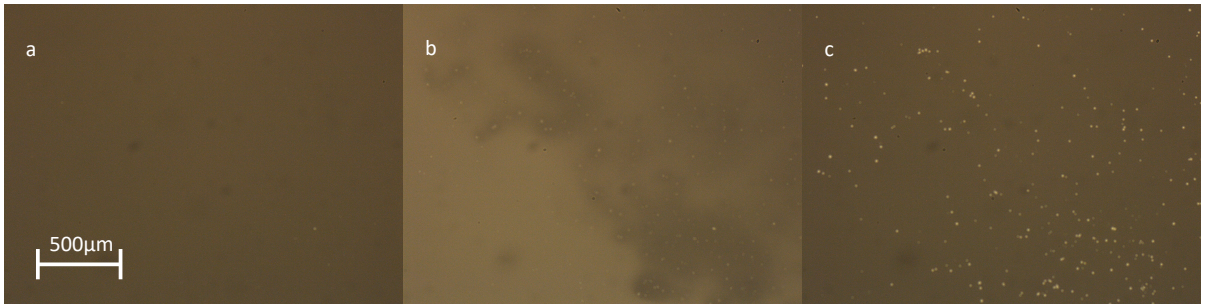

Figure 3.11: Sample of type B during three different stages of hydrogen loading. a) Before loading. The sample appears dark and homogeneous. b) Six hours into the experiment. The sample is more clear with some dark regions. White spots have started forming due to long exposure to the electrolyte. c) Twenty-four hours after the experiment. All the hydrogen has diffused out of the sample, which has returned to its original transparency. The white spots are now more visible.

Conclusions

The long-term goal of this project was to use the electrochemical method in order to be able to distinguish the role of interfaces, stresses and microstructure during hydrogen loading. Various experiments were carried out to choose the correct parameters to use during the measures, like applied voltage and loading time. We prepared different types of thin films using Ar-ion beam sputtering. The quality of such films was confirmed by performing an EDS measurement on a Pd thin film. The layer thicknesses in some sample were directly measured using XRR. The hydrogenation of these films was studied using electrochemical hydrogen loading. High currents have proven to spoil the measure with unwanted effects. Formation of magnesium hydride was observed both from the calculated composition isotherm and in-situ optical microscopy. Mg/Ti multilayers were prepared to study hydride diffusion in these systems. Data on transparency suggests that titanium hydride forms before magnesium hydride. The study on hydrogenation of Mg/Ti multilayers highlighted the limitations of the experimental setup with manual switch, which has proven to be non-practical when studying samples with higher hydrogen diffusion time. This lead to the design of a new experimental setup with an automatic relay and current provided instead of voltage. The major upside of the automatic measurement is its regularity, which allows to easily record curves at any time after the current pulse. This provides details not only on the phase transitions, but also on the speed of diffusion as the hydrogen concentration increases. For the sample of type A, with 2 layers of Ti and 1 of Mg, this method allowed to correctly estimate the following values of hydrogen concentration: H/(Mg+Ti)= 2.1 ± 0.2, H/Mg= 2.0 ± 0.2, H/Pd= 0.49 ± 0.05. For the sample of type B, with fifteen 1 nm layers of Ti and Mg alternated, the hydrogen concentration estimate was not as successful. This may be due to the fact that at some point the hydrogen diffusion in this type of sample takes longer than the 5 minutes that were set in the experiment as waiting time. More tests should be carried out with longer waiting times in order to see the differences. It was proven using both electrochemical voltage measure and in-situ optical microscopy that the hydride phases inside the sample are not stable as the hydrogen slowly diffuses back into the electrolyte. This effect puts a constraint on the waiting time set for the experiment, if the hydrogen concentration has to be accurate enough.

Appendix A

Python and TSP

The following is the Python script used to control the SMU from the PC. The connection was made using the RS232 port. The TSP command that can be read by the SMU are wrapped inside the `write()` method used by the API. A simple `for` loop and the `sleep` function are used to produce the pulses of desired length. During the waiting time the current is set to zero by the SMU.

The Python code

```
import pyvisa
from time import sleep

rm = pyvisa.ResourceManager()

keithley = rm.open_resource('ASRL1::INSTR')

# reset instrument
keithley.write('reset()')

# select current as source
keithley.write('smua.source.func = smua.OUTPUT_DCAMPS')

# set current limit to 10mA and range to 1mA
keithley.write('smua.source.limiti = 1e-3')
keithley.write('smua.source.rangei = 1e-3')

# set voltage limit to 10V
keithley.write('smua.source.limitv = 10')

# set current to 0
keithley.write('smua.source.leveli = 0.0')

```

```
24 # output on
25 keithley.write('smua.source.output = smua.OUTPUT_ON')
26
27 input('Press Enter to start')
28
29 for i in range(10):
30     keithley.write('smua.source.leveli = 0.5e-3')
31     sleep(1)
32     keithley.write('smua.source.leveli = 0')
33     sleep(300)
34
35 for i in range(40):
36     keithley.write('smua.source.leveli = 0.5e-3')
37     sleep(1)
38     keithley.write('smua.source.leveli = 0')
39     sleep(1800)
```

Appendix B

Arduino

The Arduino is programmed using this C++ script, modified from a script by Dr. P. Klose, IAM-WK. The function `pulse()` sets the switches on and off for the selected times. Repeated pulses are produced using a simple `for` loop. Once the Arduino has been programmed it can be connected to the circuit as a normal relay and switched on.

The C++ code

```
int r = 0; // Pin of the resistor to "measure" current
int k1 = 2 ; // pins of the relays
int k2 = 3 ;
int k3 = 4 ;
int k4 = 5 ;
int k5 = 6 ;
int k6 = 7 ;
void setup() {
  // put your setup code here, to run once:
  pinMode(r, INPUT); // because we want to "measure" current this has
   to be an input
  pinMode(k1, OUTPUT); // declaring pins as output
  pinMode(k2, OUTPUT);
  pinMode(k3, OUTPUT);
  pinMode(k4, OUTPUT);
  pinMode(k5, OUTPUT);
  pinMode(k6, OUTPUT);


  digitalWrite(k1,LOW);
  digitalWrite(k2,LOW);
  digitalWrite(k3,LOW);
  digitalWrite(k4,LOW);
  digitalWrite(k5,LOW);
```

```
24   digitalWrite(k6,LOW);
25 }
26
27 void pulse(){
28   digitalWrite(k4,HIGH);
29   digitalWrite(k5,HIGH);
30   digitalWrite(k6,HIGH);
31
32   delay(1000); //loading-time in ms
33
34   digitalWrite(k4,LOW);
35
36   digitalWrite(k5,LOW);
37   digitalWrite(k6,LOW);
38
39   delay(300000); //wating for equilibrium for 5 min
40 }
41 void loop() {
42   // put your main code here, to run repeatedly:
43   for(int i=0; i<100;i++){ //running over 100 cycles
44     pulse()
45   }
46   delay(86400000); //waiting 24 hours
47 }
```

Appendix C

Python functions for data analysis

The following are the Python functions developed to carry out the data analysis of the results. The functions `loading_MgTi()`, `loading_Mg()`, `loading_Pd()` are used to compute how much the ratio H/metal increases at each step, given the parameters `current` and pulse duration `t`. The function `concentration()` is then to be used to sum up all the contributions, giving the actual ratio after every pulse. The function `transmittance()` was used to compute the brightness of the pictures taken after every pulse. The relative transmittance can be computed dividing the array by the first element `t[0]`.

Python functions

```
import numpy as np
from PIL import Image

# parameters
current = 5e-4   # A
sampling_frequency = 1000 / 216   # Hz
pulses = np.ones(100)   # number of pulses in sec

# constants
faraday_number = 96485
radius_o_ring = 0.4
molar_volume_Pd = 8.85
molar_volume_Mg = 14
molar_volume_Ti = 10.62


def loading_MgTi(t, h, num_layers_Ti, num_layers_Mg):
    '''
    Compute H/metal ratio in multi-layered Ti/Mg.
    '''
```

```
    moles_Ti = np.pi * radius_o_ring ** 2 * h * num_layers_Ti /
    molar_volume_Ti
    moles_Mg = np.pi * radius_o_ring ** 2 * h * num_layers_Mg /
    molar_volume_Mg
    moles_H = current * t / faraday_number
    return moles_H / (moles_Ti + moles_Mg)


def loading_Mg(t, h):
    '''
    Compute H/Mg ratio in magnesium layer.
    '''
    moles_Mg = np.pi * radius_o_ring ** 2 * h / molar_volume_Mg
    moles_H = current * t / faraday_number
    return moles_H / moles_Mg


def loading_Pd(t, h):
    '''
    Compute H/Pd ratio in palladium layer.
    '''
    moles_Pd = np.pi * radius_o_ring ** 2 * h / molar_volume_Pd
    moles_H = current * t / faraday_number
    return moles_H / moles_Pd


def concentration(steps):
    '''
    Get H/metal ratio after a certain number of steps.
    '''
    c = np.zeros(len(steps)+1)
    c[0] = 1e-4
    for i in range(len(steps)):
        c[i+1] = c[i] + steps[i]
    return c


def transmittance(images):
    '''
    Compute average brightness of images.
    '''
    t = np.empty(len(images))
    for i, image in enumerate(images):
        with Image.open(image) as im:
            imarray = np.array(im)
        hist, bin_edges = np.histogram(imarray, bins=256)
        t[i] = np.average(bin_edges[:-1], weights=hist)
    return t
```

Bibliography

[1] EERE. 2022. URL: https://www.energy.gov/eere/fuelcells/hydrogen-storage.

[2] A. Baldi et al. "Mg/Ti multilayers: Structural and hydrogen absorption properties". In: *Phys. Rev. B* 81 (22 2010), p. 224203. DOI: 10.1103/PhysRevB.81.224203. URL: https://link.aps.org/doi/10.1103/PhysRevB.81.224203.

[3] Andreas Züttel et al. "Hydrogen: the future energy carrier". In: *Philosophical Transactions of the Royal Society A: Mathematical, Physical and Engineering Sciences* 368.1923 (2010), pp. 3329–3342.

[4] A.Pundt R.Kirchheim. *Chapter 25 - Hydrogen in Metals of Physical Metallurgy.* 5th ed. Elsevier, Oxford, 2014.

[5] H Peisl. "Lattice strains due to hydrogen in metals". In: *Hydrogen in metals I* (1978), pp. 53–74.

[6] B Baranowski, S Majchrzak, and TB Flanagan. "The volume increase of fcc metals and alloys due to interstitial hydrogen over a wide range of hydrogen contents". In: *Journal of Physics F: Metal Physics* 1.3 (1971), p. 258.

[7] E Wicke, H Brodowsky, and H Züchner. "Hydrogen in palladium and palladium alloys". In: *Hydrogen in metals II* (1978), pp. 73–155.

[8] J. F. Jr. Stampfer, C. E. Jr. Holley, and J. F. Suttle. "The Magnesium-Hydrogen System1-3". In: *Journal of the American Chemical Society* 82.14 (1960), pp. 3504–3508. DOI: 10.1021/ja01499a006. eprint: https://doi.org/10.1021/ja01499a006. URL: https://doi.org/10.1021/ja01499a006.

[9] WILLIAM M MUELLER. "Titanium hydride". In: *Metal hydrides* (1968).

[10] Yuh Fukai. *The metal-hydrogen system: basic bulk properties.* Vol. 21. Springer Science & Business Media, 2006.

[11] K. Zeng et al. "Critical assessment and thermodynamic modeling of the Mg–H system". In: *International Journal of Hydrogen Energy* 24.10 (1999), pp. 989–1004. ISSN: 0360-3199. DOI: https://doi.org/10.1016/S0360-3199(98)00132-3. URL: https://www.sciencedirect.com/science/article/pii/S0360319998001323.

[12] *Magnesium hydride - Wikipedia*. URL: https://en.wikipedia.org/wiki/Magnesium_hydride.

[13] C. W. Bale et al. *Factsage Thermochemical Software and Databases*. 2016. URL: https://www.factsage.com.

[14] Shusuke Ukita, Hiroshi Ohtani, and Mitsuhiro Hasebe. "Thermodynamic Analysis of the Ti-H and Zr-H Binary Phase Diagrams". In: *Journal of the Japan Institute of Metals and Materials* 71.9 (2007), pp. 721–729. DOI: 10.2320/jinstmet.71.721.

[15] Lennard P.A. Mooij et al. "Interface Energy Controlled Thermodynamics of Nanoscale Metal Hydrides". In: *Advanced Energy Materials* 1.5 (2011), pp. 754–758. DOI: https://doi.org/10.1002/aenm.201100316. eprint: https://onlinelibrary.wiley.com/doi/pdf/10.1002/aenm.201100316. URL: https://onlinelibrary.wiley.com/doi/abs/10.1002/aenm.201100316.

[16] Stefan Wagner and Astrid Pundt. "Quasi-thermodynamic model on hydride formation in palladium–hydrogen thin films: Impact of elastic and microstructural constraints". In: *International Journal of Hydrogen Energy* 41.4 (2016), pp. 2727–2738. ISSN: 0360-3199. DOI: https://doi.org/10.1016/j.ijhydene.2015.11.063. URL: https://www.sciencedirect.com/science/article/pii/S0360319915310272.

[17] Thomas Mütschele. *Löslichkeit und Diffusion von Wasserstoff in nanokristallinem Palladium*. M. Planck Institut, 1987.

[18] A. Pundt and R. Kirchheim. "HYDROGEN IN METALS: Microstructural Aspects". In: *Annual Review of Materials Research* 36.1 (2006), pp. 555–608. DOI: 10.1146/annurev.matsci.36.090804.094451. eprint: https://doi.org/10.1146/annurev.matsci.36.090804.094451. URL: https://doi.org/10.1146/annurev.matsci.36.090804.094451.

[19] K. Christmann. "Interaction of hydrogen with solid surfaces". In: *Surface Science Reports* 9.1 (1988), pp. 1–163. ISSN: 0167-5729. DOI: https://doi.org/10.1016/0167-5729(88)90009-X. URL: https://www.sciencedirect.com/science/article/pii/016757298890009X.

[20] T. Mütschele and R. Kirchheim. "Segregation and diffusion of hydrogen in grain boundaries of palladium". In: *Scripta Metallurgica* 21.2 (1987), pp. 135–140. ISSN: 0036-9748. DOI: https://doi.org/10.1016/0036-9748(87)90423-6. URL: https://www.sciencedirect.com/science/article/pii/0036974887904236.

[21] Stefan Wagner and Astrid Pundt. "Mechanical stress impact on thin Pd1-xFex film thermodynamic properties". In: *Applied Physics Letters* 92.5 (2008). DOI: 10.1063/1.2841636.

[22] Lev Davidovič Landau et al. *Lehrbuch der theoretischen Physik*. Vol. 1. Akademie Verlag Berlin, 1966.

[23] *The Nernst Equation*. [Online; accessed 2023-02-02]. 2022.

[24] N. Boes and H. Züchner. "Electrochemical methods for studying diffusion, permeation and solubility of hydrogen in metals". In: *Journal of the Less Common Metals* 49 (1976). Hydrogen in metals, pp. 223–240. ISSN: 0022-5088. DOI: https://doi.org/10.1016/0022-5088(76)90037-0. URL: https://www.sciencedirect.com/science/article/pii/0022508876900370.

[25] Giulio Bonelli. *Electrochemical loading of hydrogen in Mg thin films*. 2020.

[26] Giorgia Guardi. *Thickness effects on electrochemical and gas-phase hydrogen loading in magnesium thin films*. 2021.